THE ASTROPHYSICAL JOURNAL, 431:L63–L66, 1994 August 10

COBE DIRBE NEAR-INFRARED POLARIMETRY OF THE ZODIACAL LIGHT: INITIAL RESULTS

G. B. BERRIMAN,[1] N. W. BOGGESS,[2] M. G. HAUSER,[3] T. KELSALL,[2] C. M. LISSE,[4]
S. H. MOSELEY,[2] W. T. REACH,[5] AND R. F. SILVERBERG[2]
Received 1993 August 27; accepted 1994 May 24

ABSTRACT

This *Letter* describes near-infrared polarimetry of the zodiacal light at 2.2 μm, measured with the Diffuse Infrared Background Experiment (DIRBE) aboard the *Cosmic Background Explorer* (*COBE*) spacecraft. The polarization is due to scattering of sunlight. The polarization vector is perpendicular to the scattering plane, and its observed amplitude on the ecliptic equator at an elongation of 90° and ecliptic longitude of 10° declines from 12.0 $\pm$ 0.4% at 1.25 μm to 8.0 $\pm$ 0.6% at 3.5 μm (cf. 16% in the visible); the principal source of uncertainty is photometric noise due to stars. The observed near-infrared colors at this location are redder than Solar, but at 3.5 μm this is due at least in part to the thermal emission contribution from the interplanetary dust. Mie theory calculations show that both polarizations and colors are important in constraining models of interplanetary dust.

Subject headings: infrared: solar system — instrumentation: polarimeters — interplanetary medium — polarization — solar system: general — techniques: polarimetric

1. INTRODUCTION

The Diffuse Infrared Background Experiment (DIRBE) aboard the *Cosmic Background Explorer* (*COBE*) includes a liquid-helium cooled, off-axis Gregorian telescope and an absolute radiometer and polarimeter (Hauser et al. 1991; Boggess et al. 1992; Silverberg et al. 1993). Between 1989 November and 1990 September, it performed the first linear polarization survey of diffuse emission over the full sky in three photometric bands at 1.25 μm, 2.2 μm, and 3.5 μm.

This *Letter* outlines the operation of the polarimeter and presents polarization maps of the zodiacal light at 2.2 μm. The zodiacal light is 15%–20% linearly polarized in the visible (Leinert 1975), a natural consequence of its origin in sunlight scattered by interplanetary dust. DIRBE polarimetry and near-infrared colors together are powerful probes of the properties of the grains, as will be demonstrated by comparing observations at solar elongation, ϵ (the angle between the line of sight and the Sun), of 90° with the results of Mie scattering calculations. Further modeling of the polarizations and colors over the whole sky will ultimately aid in achieving the principal aim of the DIRBE of discriminating foreground radiation to search for an isotropic extragalactic background.

2. MEASUREMENT OF POLARIZATION WITH DIRBE

2.1. *Convention for Stokes Parameters*

The linear Stokes parameters Q and U are defined in ecliptic coordinates relative to the local line of longitude: Q is the component parallel (positive values) or perpendicular (negative values) to the local line of longitude; U is the component at 45° E (positive) or 45° W (negative) of the line of longitude. Both are measured as fractions of the total intensity.

2.2. *Construction and Operation of the DIRBE Polarimeter*

DIRBE simultaneously measures polarizations and intensities at 1.2, 2.2, and 3.5 μm in bandpasses that approximate the J, K, and L filters. It is equipped with a three channel polarimeter for each band. Channel "a" measures the intensity and channels "b" and "c" contain polarizers whose transmission axes are orthogonal, with the "c" channels aligned along the DIRBE scan direction on the sky. All the polarizers are fixed inside the DIRBE, which rotates as the *COBE* scans the sky, eliminating the effect of instrumental polarization on the measured sky polarizations.

Each channel contains an InSb photovoltaic detector and all share a common instantaneous 0.°7 × 0.°7 field of view. DIRBE records, at a time resolution of $\frac{1}{8}$ s, the intensities in each channel, I_a, I_b, and I_c, and the polarizer orientations, Θ, the angles between the polarizer axes and the local line of longitude. Data are accumulated over one week to obtain adequate signal-to-noise ratio in each DIRBE pixel (0.°32 × 0.°32). Because the polarizers are fixed, the sky coverage of Q and U is governed by the DIRBE scan path.

2.3. *Sky Coverage and Calculation of Q and U*

The DIRBE scan path is a helix 60° wide, maintained between $64° < \epsilon < 124°$ as depicted in Figure 1*a* (Plate L7) over four orbits of the Earth. The "c" polarizers can be visualized as tangential to the scan path and their orientations vary continuously as the DIRBE scans across the sky. Consider the orientations on the ecliptic equator. At the edges of the viewing swath, $|\Theta| \approx 0°$—the "c" polarizer is aligned north-south—and in the middle of the swath, $|\Theta| \approx 90°$. Only Q is calculable near these orientations. Similarly, only U is calculable between the middle and edges of the swath, where $|\Theta| \approx 45°$.

The spacecraft orbit precesses 1° day^{-1} to remain Sun-synchronous. Hence, over one week, more of the sky is sampled

[1] General Sciences Corporation, Code 685.3, NASA Goddard Space Flight Center, Greenbelt, MD 20771.
[2] Code 685, NASA Goddard Space Flight Center, Greenbelt, MD 20771.
[3] Code 680, NASA Goddard Space Flight Center, MD 20771.
[4] Hughes STX, Code 685.3, NASA Goddard Space Flight Center, Greenbelt, MD 20771.
[5] NAS-NRC Resident Research Associate, Code 685, NASA Goddard Space Flight Center, Greenbelt, MD 20771.

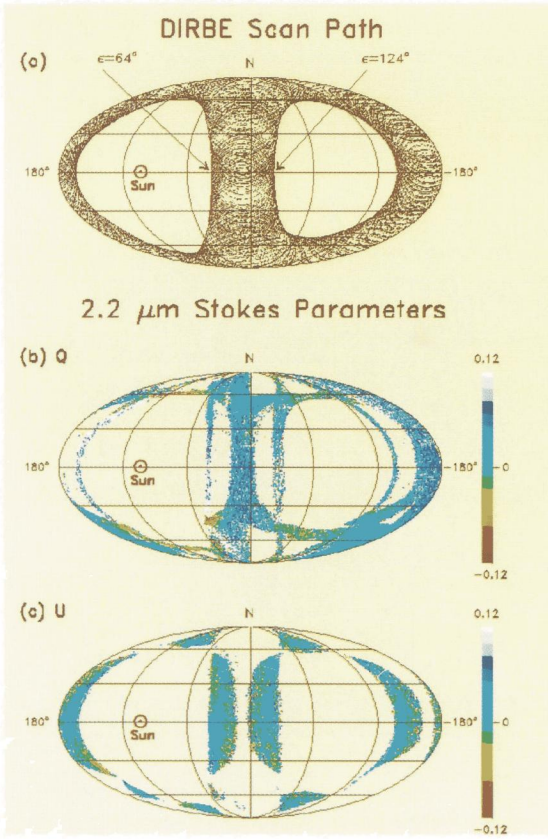

FIG. 1

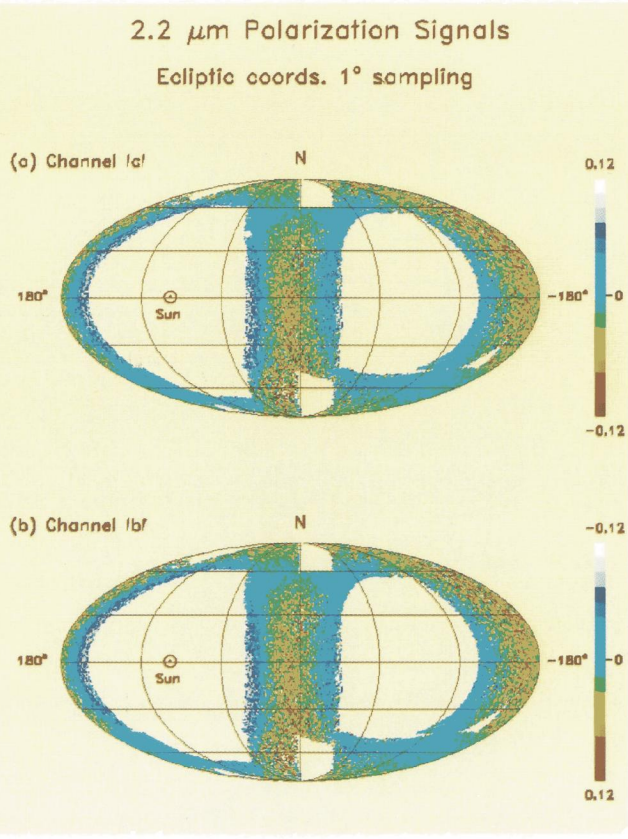

FIG. 2

FIG. 1.—(*a*) The DIRBE scan path for 1990 July 12:00–18:00 in ecliptic coordinates in a Mollweide projection. The positon of the Sun and the loci of solar elongations $\epsilon = 64°$ and 124° are shown. The figure reveals the helical path traced out by the DIRBE field of view. The polarizers in the "c" channels are always aligned along the tangent to this path. (*b*, *c*) Sky maps of the 2.2 μm Stokes parameters Q (*b*) and U (*c*), smoothed to 1° sampling in ecliptic coordinates in a Mollweide projection. Averages of values derived independently from the "b" and "c" channels for 1990 June 30–July 5 are shown. The coverage of Q and U is asymmetric about the center of the scan path because the spacecraft spin axis is tipped back from the normal to the orbital velocity vector. The two frames show how Q and U are alternately measured as DIRBE scans across the sky.

FIG. 2.—Maps at 2.2 μm in ecliptic coordinates in a Mollweide projection of the average polarization signals, Y (§ 2.3) in channels "b" and "c" from 1990 June 30 to July 5, smoothed to 1° spatial sampling, after removal of bright stars. The scales on the color bars are in opposite directions, so that the two signals can be directly compared. The plate includes only data obtained when the DIRBE field of view was moving east to west across the sky. Gaps occur where there are too few data to produce a reliable average. (*a*) Channel "c"; (*b*) channel "b."

BERRIMAN et al. (see 431, L63 & L64)

at orientations of 0°, ±45°, and 90° than is the case over four orbits. This wider sampling of orientations allows Q and U to be calculated in zones ≈8°–12° wide in elongation. For Q, two zones extend in from the edges of the scan path at $\epsilon = 64°$ and $\epsilon = 124°$, and a third is centered in the middle of the scan path at $\epsilon = 94°$. For U, the zones are centered on $\epsilon = 79°$ and 109°. Inside these zones, a range of orientations of 5° generally allows one parameter to be found by least-squares fitting (see below), while the other parameter takes on unphysically large values and very small signal-to-noise ratios. Thus in 1 week, Q and U are determined alternately as the spacecraft scans. The same remarks apply to the "b" channel, for the orthogonal "b" and "c" polarizers measure the same Stokes parameter instantaneously.

The Stokes parameters are found independently for the "c" and "b" channels through weighted least-squares fits of the form $Y = Q \cos 2\Theta + U \sin 2\Theta$. The polarization signal, Y, is defined for each channel as $Y_c = I_c/I_a - 1$ and $Y_b = 1 - I_b/I_a$. Observations of nearby, early-type calibration stars, assumed unpolarized, are used to establish the relative photometric scale for each signal. Absolute calibrations of I_a, I_b, and I_c are not necessary to determine Q and U. To produce a weekly polarization map, the two values of the determinate Stokes parameter in each pixel are averaged, and the indeterminate Stokes parameter is discarded.

3. POLARIZATION OF THE SKY AT 2.2 μm

Figures 1*b*, 1*c*, and 2 (Plate L7) present polarization maps of the diffuse sky at 2.2 μm, obtained for 1990 June 29 to July 5. Figure 2 shows the average polarization signals, Y, in ecliptic coordinates at a spatial sampling of 1°. The scale for "b" runs from negative to positive, reversed from that for "c" to show directly that the two signals are of consistent amplitude. The Stokes parameters averaged over "b" and "c" are presented in Figures 1*b* and 1*c*, where the alternate measurement of Q and U across the sky becomes obvious. The zodiacal light is the principal source of 2.2 μm polarization. The Galaxy is nearly unpolarized at 2.2 μm, and is seen as the smooth arc between ecliptic longitudes of $\lambda = \pm 60°$ near ecliptic latitude $\beta = 60°$ and as the smooth patches near $\lambda = 180°$ and $-180°$ and $\beta = -60°$.

3.1. *Polarization Characteristics of Zodiacal Light at* 2.2 μm

The important characteristics are most easily seen between latitudes of $\beta = \pm 45°$. In Figures 2*a* and 2*b*, the polarization signals change systematically from peak positive values at the edges of the viewing swath ($\Theta = 0°$) through zero to peak negative values in the middle ($\Theta = 90°$). This behavior demands that the polarization vector is aligned with the local meridian; that is, perpendicular to the scattering plane, except in the unlikely event that there is a polarization component always at 45° to the "b" and "c" polarizers and rotating with them. The amplitude of the vector declines with increasing elongation, because the polarization signals at $\epsilon = 64°$ are higher than those at $\epsilon = 124°$.

The Stokes parameters reflect these characteristics. Although nonzero values of U are seen at higher latitudes, on average $U \approx 0\%$, while $Q = +12\%$ at $\epsilon = 64°$ and $Q = +8\%$ at $\epsilon = 124°$, roughly the same rate of decline seen in the visual (Leinert 1975). Weinberg & Hahn (1968) reported a polarization "neutral point" (zero-crossing from positive to negative values) that advances from $\epsilon = 165°$ at 0.55 μm to $\epsilon = 102°$–122° at 0.8 μm. Yet the DIRBE data show no evidence for a neutral point anywhere from $\epsilon = 64°$ to 124°. Nor do they show the appreciable increase in polarization with ecliptic latitude seen in the visible (Weinberg & Hahn 1980).

3.2. *Noise in the Polarization Maps*

Stars are the principal source of short wavelength photometric noise in the large, sharp-edged DIRBE beam. Each channel has a slightly different beam pattern, so "contaminating" stars are not fully canceled when forming the intensity ratios. The effects of this imperfect cancellation vary widely from pixel-to-pixel, and lead to wide variations in the statistical uncertainties of the Stokes parameters: this is what gives rise to the mottled appearance of the maps. Generally, the fractional uncertainties σ_Q/Q and σ_U/U in one-square-degree samples at 2.2 μm are in the range of 1% to 15%, with roughly half the observed sky (excluding Galactic latitudes in the range $|b| < 7°$) having fractional statistical uncertainties of 10% or less.

4. MODELING THE INFRARED COLORS AND POLARIZATIONS

4.1. *Measured Polarizations and Colors of the Zodiacal Light*

The colors and polarizations of the zodiacal light are most reliably modeled at high Galactic latitudes in regions containing relatively few stars, so corrections for stellar and interstellar emission need not be made. Such is provided by the 1 square degree area centered on $\lambda = 10°$ and $\beta = 0°$ ($b = -60°$), measured from 1990 June 29 to July 5, when the average elongation was near 90°; the peak zodiacal brightness was at $\beta = -2.°5$. No correction has been made for isotropic extragalactic emission: Hauser et al. (1991) argued that it is inconsequential (cf. Matsumoto, Akiba, & Murakami 1988; Noda et al. 1992). As far as can be judged, the radiation from this region is attributable principally to the zodiacal light.

Table 1 reports the polarizations and colors. It presents only the Stokes parameters Q, but they equal the total polarizations because $U = 0$ in the ecliptic plane (§ 3.1). The uncertainties are attributable to sky noise arising from stars. The near-infrared colors are shown relative to the Sun, $[I_\nu(\lambda)/I_\nu(1.25\ \mu\text{m})]_\odot$, where the intensities I_ν are derived from the "a" channels. The color uncertainties are due largely to uncertainties in the absolute calibration of the "a" channels.

To model the scattered zodiacal light, the 3.5 μm sky brightness must be corrected for thermal emission from interplanetary dust. Emission at a color temperature of 250 K, the minimum value consistent with the DIRBE photometry between 5 and 240 μm (Spiesman et al. 1994), gives a secure lower limit of 7% to the thermal emission component at 3.5 μm (cf. ≤0.0001% at $\lambda \leq 2.2$ μm). Corrections for this lower limit obviously lead to a lower limit on Q and an upper limit on $[I_\nu(3.5\ \mu\text{m})/I_\nu(1.25\ \mu\text{m})]_\odot$, which are given in Table 1 and depicted along with the 1.25 and 2.2 μm data in Figures 3*a* and 3*b*.

The visible polarization remains roughly constant at 16 ± 4% from 5000 to 9000 Å (Pitz et al. 1979). Table 1 shows that the polarization is smaller at 1.25 μm and 2.2 μm, and possibly at 3.5 μm. The wavelength dependence is made clear through the inclusion of the 0.55 μm polarization in Figure 3*b*.

The red $[I_\nu(2.2\ \mu\text{m})/I_\nu(1.25\ \mu\text{m})]_\odot$ color seen by DIRBE is likely part of a progressive "reddening" that begins in the visible (Pitz et al. 1979; cf. Matsumoto et al. 1988). In the case of $[I_\nu(3.5\ \mu\text{m})/I_\nu(1.25\ \mu\text{m})]_\odot$, however, the upper limit in Figure 3*a* is such that solar colors cannot be ruled out.

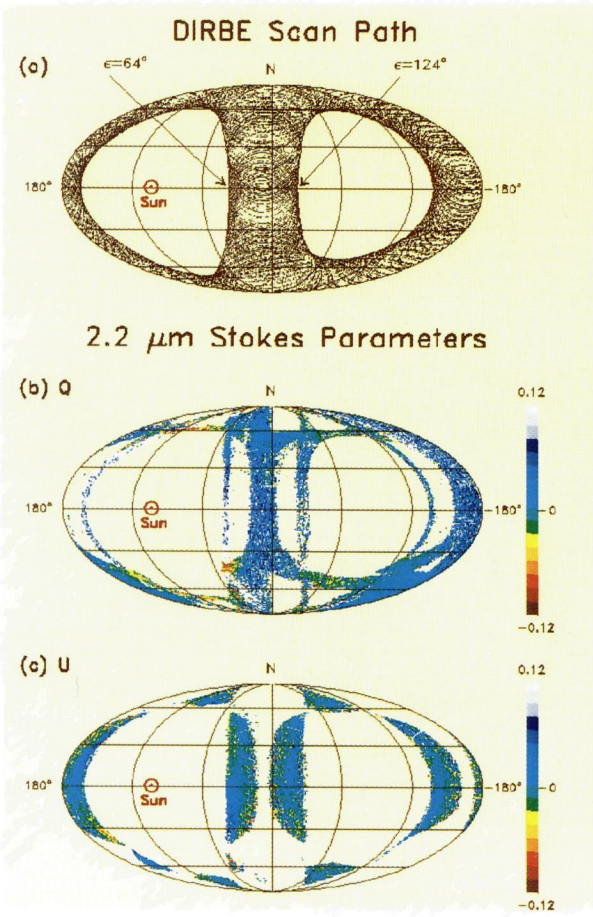

FIG. 1

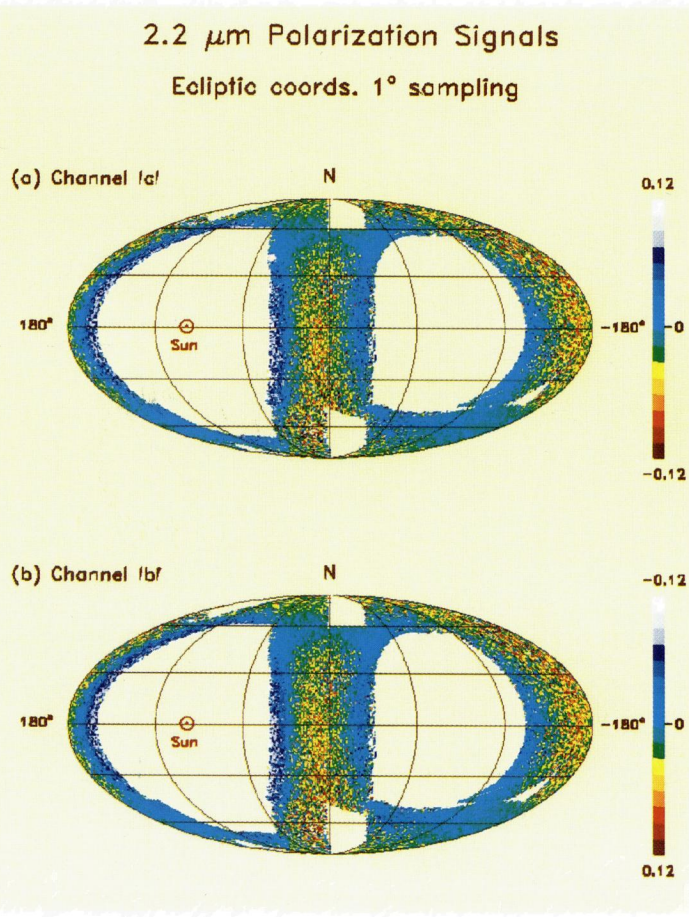

FIG. 2

FIG. 1.—(*a*) The DIRBE scan path for 1990 July 12:00–18:00 in ecliptic coordinates in a Mollweide projection. The positon of the Sun and the loci of solar elongations $\epsilon = 64°$ and 124° are shown. The figure reveals the helical path traced out by the DIRBE field of view. The polarizers in the "c" channels are always aligned along the tangent to this path. (*b*, *c*) Sky maps of the 2.2 μm Stokes parameters *Q* (*b*) and *U* (*c*), smoothed to 1° sampling in ecliptic coordinates in a Mollweide projection. Averages of values derived independently from the "b" and "c" channels for 1990 June 30–July 5 are shown. The coverage of *Q* and *U* is asymmetric about the center of the scan path because the spacecraft spin axis is tipped back from the normal to the orbital velocity vector. The two frames show how *Q* and *U* are alternately measured as DIRBE scans across the sky.

FIG. 2.—Maps at 2.2 μm in ecliptic coordinates in a Mollweide projection of the average polarization signals, Y (§ 2.3) in channels "b" and "c" from 1990 June 30 to July 5, smoothed to 1° spatial sampling, after removal of bright stars. The scales on the color bars are in opposite directions, so that the two signals can be directly compared. The plate includes only data obtained when the DIRBE field of view was moving east to west across the sky. Gaps occur where there are too few data to produce a reliable average. (*a*) Channel "c"; (*b*) channel "b."

BERRIMAN et al. (see 431, L63 & L64)

TABLE 1

NEAR-INFRARED POLARIZATION AND COLORS OF THE ZODIACAL LIGHT AT $\lambda = 10°$ AND $\beta = 0°$ WHEN $\epsilon = 90°$

λ (μm) (1)	Q (2)	Q_{corr}[1] (3)	$[I_\nu(\lambda)/I_\nu(1.25\ \mu m)]_\odot$[2] (4)	$[I_\nu(\lambda)/I_\nu(1.25\ \mu m)_{corr}]_\odot$[1,2] (5)
1.25.....	12.0 ± 0.4%	12.0 ± 0.4%	1.0	1.0
2.2.....	10.0 ± 0.5	10.0 ± 0.5	1.25 ± 0.09	1.25 ± 0.9
3.5.....	8.0 ± 0.6	>8.7	1.82 ± 0.14	<1.67

[1] Subscript "corr" denotes that values at 3.5 μm are corrected for a 7% minimum contribution from thermal emission.

[2] Colors are relative to the Sun, which has $I_\nu(2.2\ \mu m)/I_\nu(1.25\ \mu m) = 0.57$, and $I_\nu(3.5\ \mu m)/I_\nu(1.25\ \mu m) = 0.27$ (Labs & Neckel 1970).

4.2. *Modeling of the Polarizations and Colors*

The polarizations and colors of the scattered zodiacal light have been compared in Figure 3 with those of five Mie theory (spherical particle) models (Lisse 1992). The grains were assumed to be silicates or carbonaceous material, with measured refractive indices as reported by Draine & Lee (1984) and Pollack, Toon, & Khare (1973). The models assume a uniform composition and particle mass distribution along the line of sight out to 5 AU from the Earth. The number density of the grains is assumed to decline with distance, r, from the Sun as $r^{-1.3}$ (Leinert et al. 1981).

Three models are for pure silicates. One (shown as squares in Fig. 3) is for porous grains having a power law number distribution by mass of $dn/d\ \log\ m \propto m^\alpha$, where $\alpha = -0.56$, similar to models that Lisse (1992) found applicable to comets. The grains have been modeled as Bruggeman mixtures of vacuum and dust (Bohren & Huffman 1983), with density, ρ, and radius, a, related by $\rho = \rho_0(a/a_0)^{D-3}$, where $\rho_0 = 2.5$ g cm^{-3}, $a_0 = 0.1$ μm, and D, the fractal dimension, is 2.75. The other models are for "hard" grains with density $\rho_0 = 2.5$ g cm^{-3}, one (*triangles*) with the same power-law mass distribution as the porous model, and one (*diamonds*) with the interplanetary mass distribution of Grun et al. (1985), which has a broad peak centered on $a = 30$ μm.

None of the silicate models reproduce both the polarizations and the colors. Only the hard grain, power-law model can reproduce the observed polarizations. The porous model in particular has polarizations that are too high and have the

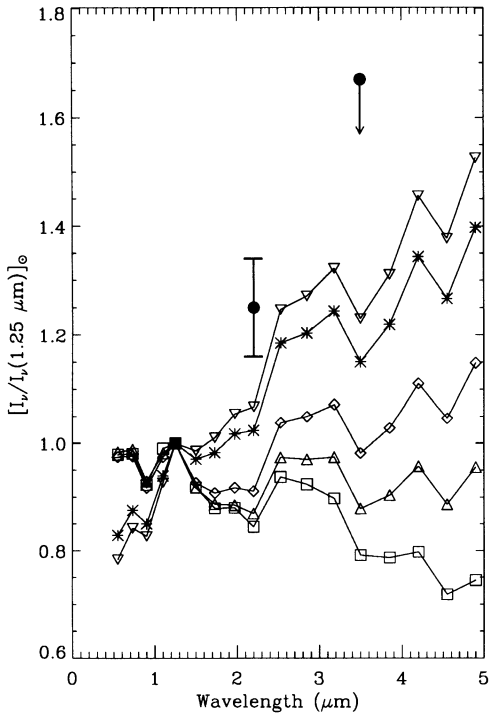

FIG. 3*a*

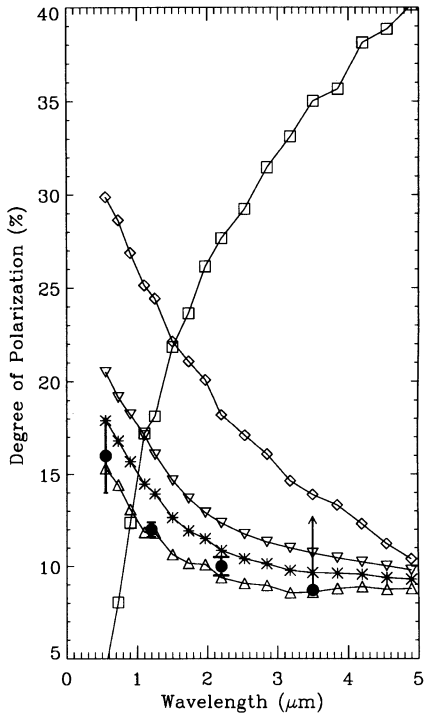

FIG. 3*b*

FIG. 3.—Comparison of (*a*) the near-infrared colors and (*b*) the polarizations of the scattered zodiacal light with those of five Mie scattering models. The oscillations apparent in the models are due to interference effects. The observations are shown as solid circles (1.2 and 2.2 μm) and arrows (limits at 3.5 μm). The visible polarimetry is from Pitz et al. (1979); the error bars represent the range given by Leinert (1975). The 3.5 μm points are limits based upon the minimum likely contribution from thermal emission, as described in the text. The models have different compositions and mass distributions indicated in the following legend. The term "power law" refers to a particle number distribution by mass of $dn/d\ \log\ m \propto m^{-0.56}$. *Squares*: porous silicates with power law. *Triangles*: hard silicates with power law. *Diamonds*: hard silicates with interplanetary dust distribution of Grun et al. (1985). *Inverted triangles*: graphite grains with power law. *Asterisks*: mixture of 50% hard silicates, 50% graphite, both with power laws.

wrong wavelength dependence. All three silicate models produce colors that are too blue in $[I_\nu(2.2\ \mu m)/I_\nu(1.25\ \mu m)]_\odot$, and possibly in $[I_\nu(3.5\ \mu m)/I_\nu(1.25\ \mu m)]_\odot$.

Models of carbonaceous material are also at odds with the data. Figure 3 shows how graphite grains with the power law number distribution (*inverted triangles*) produces polarizations that are systematically too high, and colors that are still too blue. Obviously, models with mixed composition will also disagree with the data. For example, a 50–50 mixture by mass of silicates and graphite (*asterisks*) is in better agreement with the polarizations than pure graphite, but at the expense of producing colors that are more discrepant.

While these Mie theory calculations do not reproduce the observations in detail, they do illustrate how colors and polarizations together constrain models of interplanetary dust grains. Broadly speaking, the polarizations are more sensitive to number distribution and porosity, and the colors to composition. The most likely reason why the calculations are at odds with the data (emission from e.g., a population of very small grains notwithstanding) is that interplanetary grains are rough and irregular and not smooth spheres (Giese et al. 1978; Reach 1988). Light scattered by grains with roughnesses on a scale smaller than the wavelength is redder than predicted by Mie theory (Lamy & Perrin 1991). Moreover, scattering is widely thought to be responsible for producing the $[I_\nu(2.2\ \mu m)/I_\nu(1.25\ \mu m)]_\odot$ colors of periodic comets (Hanner 1984), which are consistent with the zodiacal light colors in Table 1. Thus, models more sophisticated than those presented here are required to improve agreement with the DIRBE measurements. Such models should also use more realistic number distributions, for a power law with an index of $\alpha = -0.56$ overpredicts the number of particles larger than $\approx 10\ \mu m$ (Ceplecha 1988).

5. CONCLUSIONS

This *Letter* has described the operation of the DIRBE near-infrared polarimeter and photometer. The zodiacal light is polarized in the near-infrared, with average values at 2.2 μm of $Q = 10\%$ and $U = 0\%$. In the ecliptic plane, at an elongation of 90° and an ecliptic longitude of 10°, the observed polarization declines with increasing wavelength, and is lower than in the visible. The observed colors at this location are substantially redder than the Sun, but at 3.5 μm this is due in part to emission as well as scattering from interplanetary dust.

Mie scattering calculations show the DIRBE polarimetry and colors taken together provide strong constraints on models of the interplanetary dust. When fully developed, such models will be of value in separating the foreground diffuse infrared radiation from an isotropic cosmological component, the principal aim of the DIRBE experiment.

COBE is supported by NASA's Astrophysics Division. Goddard Space Flight Center (GSFC), under the scientific guidance of the *COBE* Science Working Group, is responsible for the development and operation of *COBE*. We wish to thank the referee, Mark Sykes, for an interesting and comprehensive report.

REFERENCES

Bohren, C. F., & Huffman, D. R. 1983, Absorption and Scattering of Light By Small Particles (New York: Wiley)
Boggess, N. W., et al. 1992, ApJ, 397, 420
Ceplecha, Z. 1988, Bull. Astron. Inst. Czech., **39**, 221
Draine, B. T., & Lee, H. M. 1988, ApJ, 285, 89
Giese, R. H., Weiss, K., Zerull, R. H., & Ono, T. 1978, A&A, 65, 365
Grun, E., Zook, H. A., Fechtig, H., & Giese, R. H. 1985, Icarus, 62, 244
Hanner, M. S. 1984, Adv. Space Res., 4, no. 9, 189
Hauser, M. G., et al. 1991, in AIP Conf. Proc. 222, After The First Three Minutes, ed. S. S. Holt, C. L. Bennett, & V. Trimble (New York: AIP), 161
Labs, D., & Neckel, H. 1970, Sol. Phys., 15, 79
Lamy, P. L., & Perrin, J. M. 1991, in Origin and Evolution of Interplanetary Dust, ed. A. C. Levasseur-Regourd & H. Hasegawa (Dordrecht: Kluwer), 163
Leinert, C. 1975, Space Sci. Rev., 18, 281
Leinert, C., Ruchter, I., Pitz, E., & Planck, B. 1981, A&A, 103, 177
Lisse, C. M. 1992, Ph.D. thesis, Univ. Maryland
Matsumoto, T., Akiba, M., & Murakami, H. 1988, ApJ, 322, 575
Noda, M., Christov, V. V., Matsuhara, H., Matsumoto, T., Matsuura, K., Noguchi, K., & Murakami, H. 1992, ApJ, 391, 456
Pitz, E., Leinert, C., Schulz, A., & Link, H. 1979, A&A, **74**, 15
Pollack, J. B., Toon, O. B., & Khare, B. N. 1973, Icarus, 19, 372
Reach, W. T. 1988, ApJ, 335, 468
Silverberg, R. F., et al. 1993, in Proc. SPIE Conf. Infrared Spaceborne Remote Sensing, ed. M. S. Scholl (SPIE), 180
Spiesman, W. J., et al. 1994, ApJ, submitted
Weinberg, J. L., & Hahn, R. C. 1968, ApJ, 152, 665
———. 1980, in Solid Particles In the Solar System, ed. I. Halliday & B. I. McIntosh (Dordrecht: Reidel), 19